RSC Advances

PAPER

View Article Online
View Journal | View Issue

Cite this: *RSC Adv.*, 2017, **7**, 512

On the stability of lithocholate derivative supramolecular tubules†

M. Gubitosi,[ab] A. D'Annibale,[a] K. Schillén,[b] U. Olsson,[b] N. V. Pavel[a] and L. Galantini*[a]

Received 31st October 2016
Accepted 26th November 2016

DOI: 10.1039/c6ra26092f

www.rsc.org/advances

The self-assembly of a mannose-labelled bile salt derivative gives rise to a metastable nematic phase of monodisperse nanotubes in aqueous solutions that are characterized by a crystalline order. This work is addressed to study the relative stability of these tubular aggregates in order to have full control of such a system for possible applications. By using a static light scattering method we evaluate both the solubilities of the metastable nanotubes and of stable nanocrystals, demonstrating that these are remarkably lower than the critical micellar concentration of typical bile salts and other ionic conventional surfactants. A partial stability map is developed by combining solubility and calorimetry data, where a nematic nanotube phase region is highlighted below 60–65 °C.

Introduction

Self-assembly has been largely considered in the last decades to be a ubiquitous strategy for the fabrication of structures of controlled morphology in the nanometer scale.[1–3] The stability of these structures is a fundamental issue for their functionality, and it has been widely investigated within both fundamental and applied research. In many cases, the ultimate goal of the fabrication is not necessarily to produce thermodynamically stable materials, as kinetically trapped structures can maintain functionality within the desired timescales and achieve the desired function. The knowledge of the non-equilibrium stability of these systems is therefore required. Solubility of these nanostructures establishes the low concentration boundary of their colloid phase region and it is strictly related to their stability to ripening. High or low soluble colloidal particles are requested depending on the applications. In the formulation of poorly soluble drugs, the reduction of organic drugs into small particles (amorphous or crystalline) is often performed as it increases the drug dissolution rate and therefore its bioavailability.[4–11]

Supramolecular tubular nanoparticles are unique structures formed by molecular self-assembly,[12] which can be employed in several nanotechnological applications such as drug-delivery[13–16] and preparation of aligned nanomaterials[17,18] and metal nanowires.[19,20] The ability to self-assemble in tubules is shared by a variety of molecules such as peptides,[21–26] phospholipids,[16,27] polymers,[28] glycolipids,[29] and rationally designed amphiphiles[30–33] giving rise in some cases to very ordered semi-crystalline structures.[32]

Another class of organic molecules particularly prone to form tubular assemblies with high degree of monodispersity is represented by bile salts (BSs), which are biological surfactants with a rigid and peculiar amphiphilic structure (Fig. 1).[34,35] A stiff steroidal backbone determines a low number of conformational degrees of freedom for their molecules[36] and allows such surfactants self-organize in ordered supramolecular architectures. Nanotubes with diameters spanning a wide range of dimensions, from hundreds[37] to few nm,[38,39] have been obtained from bile salts and their derivatives. In some cases,

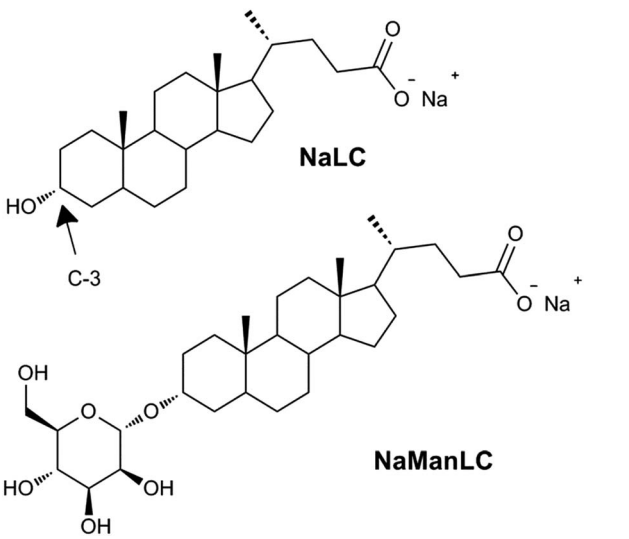

Fig. 1 Molecular structures of NaLC and its derivative NaManLC, obtained by substituting the hydroxyl group in position C-3 of the steroidal skeleton of the natural precursor with a mannose unit.

[a]*Department of Chemistry, "Sapienza" University of Rome, P.le Aldo Moro 5, 00185 Rome, Italy. E-mail: luciano.galantini@uniroma1.it*

[b]*Division of Physical Chemistry, Department of Chemistry, Lund University, SE-221 00 Lund, Sweden. Fax: +46 31 27 61 30; Tel: +46 31 706 63 81*

† Electronic supplementary information (ESI) available: The DSC thermogram of the natural bile salt precursor NaLC. See DOI: 10.1039/c6ra26092f

interesting systems providing stimuli responsive[40–42] or controlled charge tubules have been also identified.[43]

In particular, a natural bile salt, sodium lithocholate (NaLC),[44,45] and its mannose-labeled derivative, NaManLC (Fig. 1),[46] have been observed to form nanotubes in aqueous alkaline conditions. Thanks to their biological origin these nanotubes could have a significant additional potential in application. However, as NaManLC nanotubes seem to be kinetically trapped self-assembled structures, a deep knowledge of their stability is required to have full control in the applications.

To obtain this information we addressed here a study on NaManLC tubules by combining differential scanning calorimetry (DSC) and solubility data. The solubility was analyzed by using a method based on static light scattering (SLS) intensity measurements.[11] The method was recently described as a particularly convenient way to estimate the solubility gain of poorly water-soluble drug amorphous nanopowders with respect to the crystalline ones. A similar approach was employed in this work to evaluate the solubility of metastable nanotubules and nanocrystals and therefore the low concentration boundary of their colloidal phase region. The whole study allowed for a description of the phase map for metastable nanotubes and nanocrystal dispersions, thus providing fundamental information for the application of these nanostructures.

Experimental

Materials and methods

The synthesis of the derivative NaManLC has been reported elsewhere.[46] 10.0 mM samples of NaManLC in aqueous solutions of NaOH (Carlo Erba Reagents) at pH 12.0 were prepared. The solubilization of NaManLC was promoted by heating the samples at pH 12.0 up to the boiling point.

Differential scanning calorimetry

Differential scanning calorimetry (DSC) measurements were carried out using a VP-DSC differential scanning calorimeter (MicroCal, Northampton, MA). More information of the instrument can be found elsewhere.[47] Approximately 0.5 mL of sample and water (as standard sample) were injected into the sample and reference cells (made from tantalum alloy), respectively. The sample was equilibrated for 20 min at 10 °C before starting the measurements. Four up-scan and four down-scan measurements in the range of 10–90 °C with scan rate of 60 °C h^{-1} were carried out. After each first scan, the sample was equilibrated for 20 min before starting the following scan. To collect and analyze DSC data, Origin software supplied by the manufacturer was used.

Static light scattering

The setup used for the SLS measurements was an ALV/DLS/SLS-5022F, CGF-8F-based compact goniometer system from ALV-GmbH, Langen, Germany. A more detailed description of the instrument can be found elsewhere.[48] The light source was a 22 mW He–Ne laser (632.8 nm) and the laser intensity was varied using a software-controlled attenuator. A vertical polarization was achieved using a Glan laser polarizer prism with a polarization ratio better than 10^5 in front of the high-temperature cell housing. The cylindrical scattering cells of borosilicate glass with a diameter of 5 mm were immersed in a thermostated vat filled with a refractive index matched liquid (*cis*-decahydronaphthalene). In our experiments, the temperature was kept at 25.0 and 40.0 ± 0.1 °C by a Julabo heating water circulator and the solvent used for the dilutions was filtered with pores of 0.2 μm. The unpolarized scattered light was collected at 90 degrees using a detection unit that included a near-monomodal optical fiber and two high-quality avalanche photodiodes placed in a pseudo-cross geometry. The average of five consecutive measurements was reported for each concentration.

Cryo-TEM

The vitrification of the cryo-TEM sample was carried out using a controlled environment vitrification system, CEVS,[49] keeping the relative humidity close to saturation at around 26 °C. A 5 μL drop of the sample was placed on a lacey carbon-coated copper grid, made hydrophilic using a Emitech glow discharge unit, and the excess fluid was gently blotted away leaving a thin film of the gel covering the grid. The grid was then rapidly vitrified by plunging into liquid ethane (−180 °C) and stored in liquid nitrogen before the examination. The micrographs were recorded using a Philips CM120 Bio TWIN electron microscope equipped with a Gatan MSC791 cooled-CCD camera detection system, operating at 120 kV, under low electron dose conditions.

Wide-angle X-ray scattering

Wide-angle X-ray scattering (WAXS) measurements were performed on the Ganesha SAXSlab instrument (JJ X-ray, Skovlunde, Denmark). The instrument had a 2D 300k Pilatus detector from Dectris (Dectris Ltd., Baden, Switzerland) and a Genix 3D X-ray Source (Xenocs SA, Sassenage, France). The X-ray wavelength λ was 1.54 Å. The scattered curves, recorded covering the q-values up to 2.9 $Å^{-1}$ ($q = (4\pi \sin\theta)/\lambda$, where 2θ is the scattering angle), were corrected for solvent and capillary contributions. Temperature was controlled to be 25 °C with Julabo heating water circulator, having an accuracy of 0.1 °C.

Results and discussion

NaManLC was very poorly soluble in water even at high pH (12.0), where the carboxylic group is deprotonated. However, the solubilization could be promoted by heating. When cooled down to 20 °C, the sample was trapped in metastable slightly turbid viscous solutions for concentrations above 5.0 mM, which were stable for more than six months. These samples, as shown by cryo-TEM in Fig. 2, are constituted of nematic phases of highly monodisperse tubules with cross section diameters of about 20 nm, and showed birefringence when analyzed between crossed polarizers.[46] The formation of a nematic phase has been reported for natural BSs as well.[50–52] The natural precursor NaLC itself formed nematic viscous solutions in the same

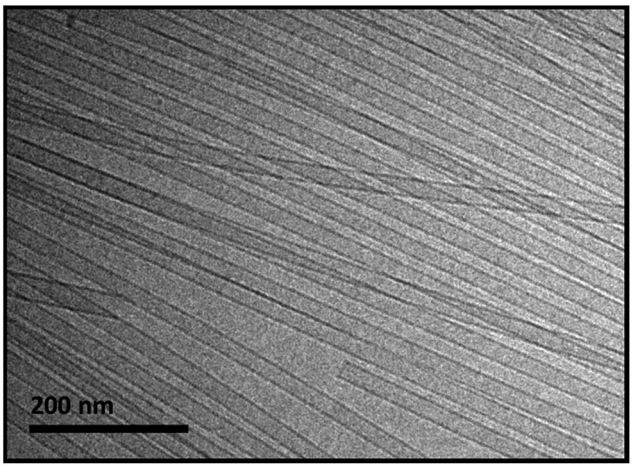

Fig. 2 Cryo-TEM images of a 10.0 mM NaManLC sample at pH 12.0 equilibrated for two weeks.

experimental conditions of concentration and pH.[44,45,53] WAXS patterns of NaManLC tubules resulted in one broad peak composed of two unresolved peaks at around 10.5 nm^{-1}. This signal was ascribed to the average molecular separation in the tube wall.[46,54]

Sonication

A 60 min sonication was applied to the viscous samples. Ice was added to the sonication bath in order to keep the temperature below 35 °C. This led to the formation of turbid nanosuspensions that exhibited no birefringence. The WAXS curve of a sonicated sample was compared with the one of crystals, obtained by evaporation of solvent from a NaManLC solution in methanol, and both are reported in Fig. 3. Such comparison established that, after sonication, the tubular aggregates experienced a rearrangement into crystals, since all the solid periodicities were restored. Therefore, dispersion of crystals was obtained by sonicating tubular metastable structures. To visualize the crystal nanosuspension, cryo-TEM images were collected. They displayed elongated particles with lengths usually smaller than 1 μm (Fig. 4).

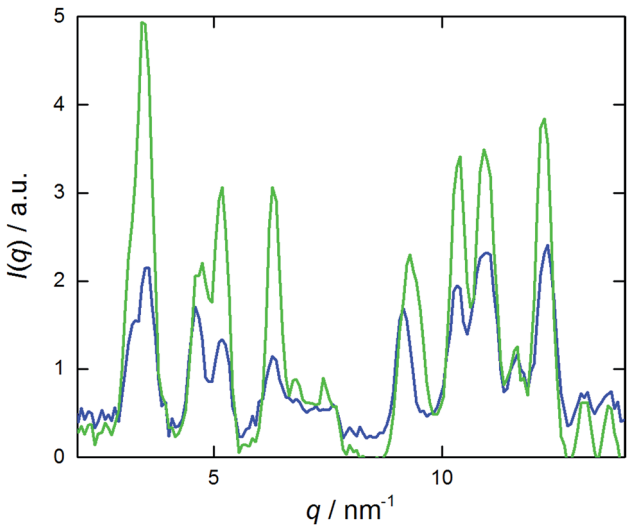

Fig. 3 WAXS patterns of crystalline (green) and sonicated (blue) 10.0 mM NaManLC samples (pH 12.0).

Solubility study

Solubility studies of crystalline dispersions (the stable phase) and tubular solutions (the metastable phase) were carried out at both 25 and 40 °C by employing a method based on the measurement of the total light scattering from colloidal nanosuspensions.[11] The basic idea of this experiment was that at concentrations below the solubility, the solutions essentially do not scatter light, while, above the solubility, the scattered light has an intensity that increases with increasing number and/or sizes of the particles (crystals or tubes) formed in the system.

The solubility was determined from the onset of intensity increase. Samples of different NaManLC concentrations were prepared by dilution of a concentrated stock solution of tubules (10.0 mM). A portion of such stock solution of NaManLC was transformed into crystal nanosuspensions by sonication and then diluted to different concentrations for the estimation of the crystal solubility. The static light scattering intensity I_{SLS} was recorded at $\theta = 90°$. The results were presented in Fig. 5, where I_{SLS} was plotted as a function of the BS derivative concentration. The onsets of the increase in the I_{SLS} patterns of the crystals and tubules occurred at 10 ± 2 and 40 ± 2 μM, respectively, at 25 °C. This suggested that a metasolubility of NaManLC was reached by diluting the latter at a concentration which was significantly higher than the crystal solubility, as generally expected for comparisons of stable and metastable nanoparticles. Moreover, the obtained values were significantly lower (approx. two orders of magnitude) than the typical critical aggregation concentration of bile salts[55,56] and other ionic conventional surfactants.[57] The measurements carried out at 40 °C exhibited breaks in the intensity curves at 25 ± 2 μM and 0.2 ± 0.02 mM for crystals and tubules, respectively. These results highlighted a widening of the difference in solubility for crystals and tubular aggregates, which probably goes in parallel with an increase of the difference in their stability, with increasing the temperature.

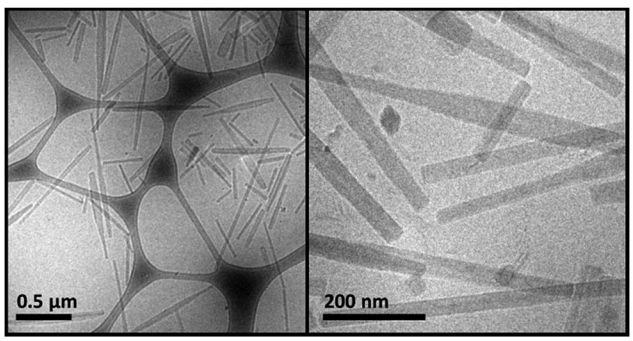

Fig. 4 Cryo-TEM images at different magnifications of a sonicated NaManLC sample. The sample at a concentration of 10.0 mM and pH 12.0 was equilibrated for two weeks and then sonicated for 60 min.

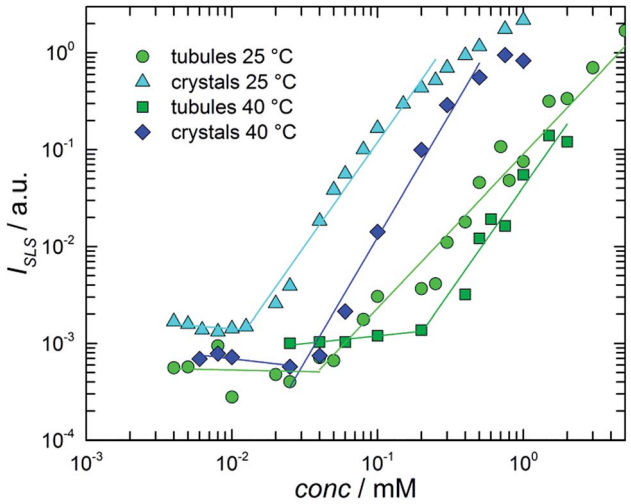

Fig. 5 Measured scattering intensity I_{SLS} as a function of NaManLC total concentration for crystalline suspensions at 25 (cyan triangles) and 40 °C (blue diamonds), and dispersions of tubules at 25 (green circles) and 40 °C (dark green squares).

Indeed, supersaturation, defined as the ratio between the solubility of the tubules and that of the crystals, could represent an indication of the width of the metastability region of the tubules in the stability map, and hence could be related to the kinetics of the transition from the metastable phase (tubules) to the stable one (crystals). We anticipated that the transition is faster the bigger the supersaturation. By increasing the temperature from 25 to 40 °C, both the solubilities increased, but the tubule solubility increased more. This means that the supersaturation increased with temperature, and hence that at higher temperatures, tubules had a higher tendency to evolve into crystals.

The birefringence, which was analyzed in order to verify the presence of tubules in the samples obtained upon dilution of the stock 10.0 mM solutions, was observed down to a concentration of 1.0 mM at 25 °C, confirming that tubules were stable in spite of the dilution. A loss of birefringence occurred at lower concentrations (*i.e.*, <1.0 mM). This was related to a transition of the tubular phase from nematic to isotropic. In a system of ideal rods with length L, diameter D and volume fraction ϕ_{tube}, a phase boundary region, based on the Onsager theory,[58,59] between isotropic and nematic phases is expected within $\phi_{tube}L/D = 3.34$ and 4.49, because of the balance of translational and orientational entropy.[60]

Considering a negligible contribution of free monomers (estimated solubility of 40 μM), the tubule volume fraction ϕ_{tube} could be roughly calculated at a concentration of 1.0 mM (≈0.00054 wt%) under the approximation of tubules with thin walls, as $\phi_{tube} \approx (R/2\delta)$ wt% $= 1.39 \times 10^{-3}$, where R is the average radius of the tubule (8.5 nm) and δ the thickness of the wall (1.8 nm).[46] By considering this value, the agreement with the Onsager nematic–isotropic boundary condition was achieved for aspect ratios > 300, which was consistent with long tubules (>6 μm) as those visible from the cryo-TEM micrographs.[46]

Temperature dependence and partial stability map

The thermal stability of dispersions of tubules at NaManLC concentrations of 5.0 and 10.0 mM was visually monitored in a thermostated oil bath. As the determination of the Krafft point was carried out in a plugged vial, the pressure was not constant in all the experiments, as high temperatures involved high pressures. The increase in the temperature promoted a first transition at around 65 °C, where the separation of a white precipitate was observed. The latter was solubilized at temperatures in the range 160–170 °C, which was identified as the Krafft temperature region. The Krafft temperatures were confirmed by using the same method on dispersions of crystals at NaManLC concentration of 1.0, 5.0 and 10.0 mM. For a deeper insight into such processes, differential scanning calorimetry (DSC) measurements were performed on a 10.0 mM viscous dispersion of tubules. The thermograms are reported in Fig. 6. Four up- and down-scans were performed on the same sample to observe their evolution in several temperature loops. The analysis of the thermograms could not allow for a proper subtraction of the background, hence raw data were reported.

The first up-scan profile exhibited a broad endothermic peak in the range 60–80 °C, outlining a first transition that involved the breakage of the tubules. The peak was reproduced in the down-scan. In the successive up- and down-scans, the same peaks were detected, but with lower and lower intensities at each scan. Moreover, a shift towards lower temperatures for the down-scan peaks was observed. We anticipated that the breaking of the tubules, *i.e.*, the metastable phase, led to a supersaturated solution of monomers that contained some crystals as well. Hence, in the successive down-scan, tubules could be formed again due to this condition of supersaturation, but in a smaller amount. The following loops of rising and decreasing of temperature endorsed more and more the nucleation of crystals, to the detriment of the tubules, which were progressively consumed. The thermogram related to the natural precursor, taken for comparison, showed also a broad

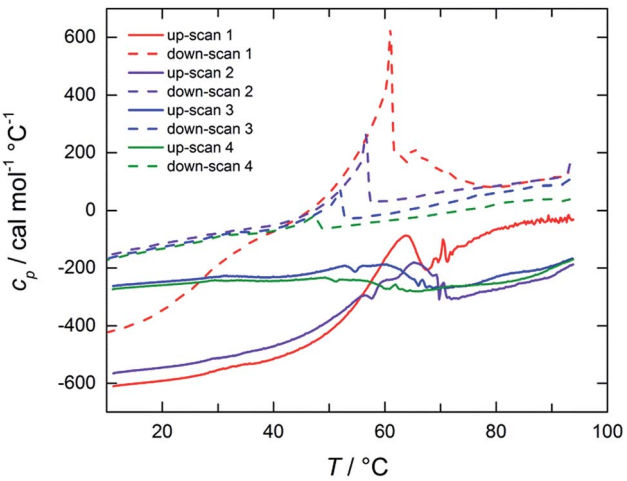

Fig. 6 Raw DSC thermograms of a 10.0 mM NaManLC sample (pH 12.0). Up-scans (solid lines) and down-scans (dashed lines) are obtained with a scan rate of 60 °C h^{-1} on the same sample.

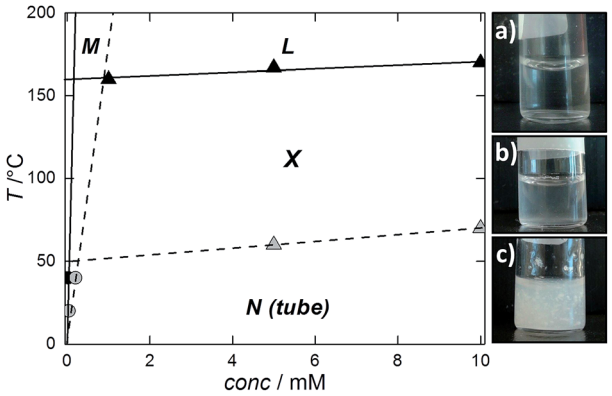

Fig. 7 Partial stability map of the NaManLC/NaOH aqueous system. Here M denotes the presence of the compound as monomer in solution, L stands for an isotropic solution of micelles (a), N for a nematic metastable phase of tubules (b), and X is related to the presence of crystals (c). Please note that the pressure is not constant (see text). Grey and black circles represent the solubility values obtained by SLS for tubules and crystals, respectively. Grey triangles are related to the breakage of the tubules outlined by DSC. Black triangles are the Krafft points for crystals in the aqueous medium at different NaManLC concentrations.

endothermic peak, but at lower temperatures (20–40 °C) than that of the NaManLC sample (Fig. S1†). The peak was related to the solubilization of the tubules that the precursor is also known to form.

A partial stability map could be sketched by reporting the visually determined Krafft points and the solubility data (from SLS) for the crystals in a *T vs.* NaManLC concentration plane (Fig. 7). The typical pattern of surfactants was obtained, with an almost vertical line representing the phase boundary between the region of the monomer solution and that of the crystals in the aqueous medium, and an almost horizontal line separating the latter phase from the micellar liquid one (L).

Within this map, a region with a similar shape at significantly lower temperatures could be outlined for the nematic metastable tubular phase (N) by plotting the solubilities and the tubule-to-crystal transition conditions highlighted by DSC.

Conclusions

A bolaamphiphilic derivative of the natural bile salt sodium lithocholate was described to form a metastable nematic phase of monodispersed tubules, which showed crystalline order in the arrangements of the molecules in the 2D walls. Such a unique system was characterized in order to obtain a picture of the relative stabilities of the metastable tubular region and the stable phase, nanocrystals.

Static light scattering method demonstrated that the metastable nanotubes formed by NaManLC were stable to dilution and showed a solubility of tens of micromolar at room temperature. Such a value, significantly lower than the critical aggregation concentration of typical bile salts, indicates that nanotubes were preserved upon dilution to very low concentrations, thus providing encouraging information about their stability and potential employment in applications.

The nanotubes showed a slightly higher solubility than the nanocrystals, which is consistent with their lower stability. The solubility of the nanotubes increased with the temperature more prominently than that of the nanocrystals. Probably strictly related to this behavior, a transition from nanotubes to supersaturated dispersion of crystals was observed around 60–65 °C.

Acknowledgements

We thank Gunnel Karlsson for the skillful assistance with the cryo-TEM experiments and Thiago Heiji Ito for the discussion about DSC.

Notes and references

1 G. M. Whitesides and B. Grzybowski, *Science*, 2002, **295**, 2418.
2 L. C. Palmer, Y. S. Velichko, M. O. de la Cruz and S. I. Stupp, *Philos. Trans. R. Soc., A*, 2007, **365**, 1417.
3 S. I. Stupp, M. U. Pralle, G. N. Tew, L. M. Li, M. Sayar and E. R. Zubarev, *MRS Bull.*, 2000, **25**, 42.
4 C. Lipinski, *J. Pharmacol. Toxicol. Methods*, 2000, **44**, 235.
5 S. H. Yalkowsky, *Solubility and Solubilization in Aqueous Media*, Oxford University Press, New York, 1990.
6 K. P. Kumar and K. G. Krishna, *Int. J. Drug Delivery*, 2011, **3**, 546.
7 V. K. Singh, D. Chandra, P. Singh, S. Kumar and A. P. Singh, *International Journal of Current Trends in Pharmaceutical Research*, 2013, **1**, 277.
8 P. Gassman, M. List, A. Schweitzer and H. Sucker, *Eur. J. Pharm. Biopharm.*, 1994, **40**, 64.
9 D. Horn and J. Rieger, *Angew. Chem., Int. Ed.*, 2001, **40**, 4330.
10 L. Lindfors, S. Forssén, P. Hedberg, U. Skantze, M. Rasmusson, A. Zackrisson and U. Olsson, *Langmuir*, 2006, **22**, 906.
11 L. Lindfors, S. Forssén, P. Skantze, U. Skantze, A. Zackrisson and U. Olsson, *Langmuir*, 2006, **22**, 911.
12 T. Shimizu, M. Masuda and H. Minamikawa, *Chem. Rev.*, 2005, **105**, 1401.
13 A. Bianco, K. Kostarelos and M. Prato, *Curr. Opin. Chem. Biol.*, 2005, **9**, 674.
14 A. Wakasugi, M. Asakawa, M. Kogiso, T. Shimizu, M. Sato and Y. Maitani, *Int. J. Pharm.*, 2011, **413**, 271.
15 K. Margulis-Goshen, M. C. di Gregorio, N. V. Pavel, L. Abezgauz, D. Danino, J. Vázquez Tato, V. H. Soto Tellini, S. Magdassi and L. Galantini, *Phys. Chem. Chem. Phys.*, 2013, **15**, 6016.
16 J. M. Schnur, *Science*, 1993, **262**, 1669.
17 R. Lv, A. Cao, F. Kang, W. Wang, J. Wei, J. Gu, K. Wang and D. Wu, *J. Phys. Chem. C*, 2007, **111**, 11475.
18 O. Carny, D. E. Shalev and E. Gazit, *Nano Lett.*, 2006, **6**, 1594.
19 B. Yang, S. Kamiya, Y. Shimizu, N. Koshizaki and T. Shimizu, *Chem. Mater.*, 2004, **16**, 2826.
20 K. Hirahara, K. Suenaga, S. Bandow, H. Kato, T. Okazaki, H. Shinohara and S. Iijima, *Phys. Rev. Lett.*, 2000, **85**, 5384.

21 M. R. Ghadiri, J. R. Granja, R. A. Milligan, D. E. McRee and N. Khazanhovic, *Nature*, 1993, **366**, 324.
22 D. T. Bong, T. D. Clark, J. R. Granja and M. R. Ghadiri, *Angew. Chem., Int. Ed.*, 2001, **40**, 988.
23 Y. Liang, S. V. Pingali, A. S. Jogalekar, J. P. Snyder, P. Thiyagarajan and D. G. Lynn, *Biochemistry*, 2008, **47**, 10018.
24 K. Lu, J. Jacob, P. Thiyagarajan, V. P. Conticello and D. G. Lynn, *J. Am. Chem. Soc.*, 2003, **125**, 6391.
25 C. Cenker, P. H. H. Bomans, H. Friedrich, B. Dedeglu, V. Aviyente, U. Olsson, N. A. J. M. Sommerdijk and S. Bucak, *Soft Matter*, 2012, **8**, 7463.
26 C. Valéry, F. Artzner and M. Paternostre, *Soft Matter*, 2011, **7**, 9583.
27 J. M. Schnur, B. R. Ratna, J. V. Selinger, A. Singh, G. Jyothi and K. R. K. Easwaran, *Science*, 1994, **264**, 945.
28 L. Cheng, G. Zhang, L. Zhu, D. Chen and M. Jiang, *Angew. Chem., Int. Ed.*, 2008, **47**, 10171.
29 K. Yoshida, H. Minamikawa, S. Kamiya, T. Shimizu and S. Isoda, *J. Nanosci. Nanotechnol.*, 2007, **7**, 960.
30 Y.-A. Lin, A. G. Cheetham, P. Zhang, Y.-C. Ou, Y. Li, G. Liu, D. Hermida-Merino, I. W. Hamley and H. Cui, *ACS Nano*, 2014, **8**, 12690.
31 E. Lee, J.-K. Kim and M. Lee, *Angew. Chem., Int. Ed.*, 2009, **48**, 3657.
32 M. R. J. Vos, P. E. L. G. Leclère, H. Meekes, E. Vlieg, R. J. M. Nolte and N. A. J. M. Sommerdijk, *Chem. Commun.*, 2010, **46**, 6063.
33 H.-Y. Lee, H. Oh, J. H. Lee and S. R. Raghavan, *J. Am. Chem. Soc.*, 2012, **134**, 14375.
34 D. Madenci and S. U. Egelhaaf, *Curr. Opin. Colloid Interface Sci.*, 2010, **15**, 109.
35 L. Galantini, M. C. di Gregorio, M. Gubitosi, L. Travaglini, J. Vázquez Tato, A. Jover, F. Meijide, V. H. Soto Tellini and N. V. Pavel, *Curr. Opin. Colloid Interface Sci.*, 2015, **20**, 170.
36 J. N. Israelachvili, D. J. Mitchell and B. W. Ninham, *J. Chem. Soc., Faraday Trans. 2*, 1979, **72**, 1525.
37 V. H. Soto Tellini, A. Jover, F. Meijide, J. Vázquez Tato, L. Galantini and N. V. Pavel, *Adv. Mater.*, 2007, **19**, 1752.
38 L. Travaglini, A. D'Annibale, K. Schillén, U. Olsson, S. Sennato, N. V. Pavel and L. Galantini, *Chem. Commun.*, 2012, **48**, 12011.
39 L. Travaglini, A. D'Annibale, M. C. di Gregorio, K. Schillén, U. Olsson, S. Sennato, N. V. Pavel and L. Galantini, *J. Phys. Chem. B*, 2013, **117**, 9248.
40 L. Galantini, C. Leggio, A. Jover, F. Meijide, N. V. Pavel, V. H. Soto Tellini, J. Vázquez Tato, R. Di Leonardo and G. Ruocco, *Soft Matter*, 2009, **5**, 3018.
41 M. C. di Gregorio, N. V. Pavel, A. Jover, F. Meijide, J. Vázquez Tato, V. H. Soto Tellini, A. Alfaro Vargas, O. Regev, Y. Kasavi, K. Schillén and L. Galantini, *Phys. Chem. Chem. Phys.*, 2013, **15**, 7560.
42 M. C. di Gregorio, M. Varenik, M. Gubitosi, L. Travaglini, N. V. Pavel, A. Jover, F. Meijide, O. Regev and L. Galantini, *RSC Adv.*, 2015, **5**, 37800.
43 N. Manghisi, L. Galantini, C. Leggio, A. Jover, F. Meijide, N. V. Pavel, V. H. Soto, J. Vázquez Tato and R. Agostino, *Angew. Chem., Int. Ed.*, 2010, **49**, 6604.
44 X. Zhang, J. Zou, K. Tamhane, F. F. Kobzeff and J. Fang, *Small*, 2010, **6**, 217.
45 B. Jean, L. Oss-Ronen, P. Terech and Y. Talmon, *Adv. Mater.*, 2005, **17**, 728.
46 M. Gubitosi, L. Travaglini, A. D'Annibale, N. V. Pavel, J. Vázquez Tato, M. Obiols-Rabasa, S. Sennato, U. Olsson, K. Schillén and L. Galantini, *Langmuir*, 2014, **30**, 6358.
47 D. Löf, A. Niemiec, K. Schillén, W. Loh and G. A. Olofsson, *J. Phys. Chem. B*, 2007, **111**, 5911.
48 J. Janiak, S. Bayati, L. Galantini, N. V. Pavel and K. Schillén, *Langmuir*, 2012, **28**, 16536.
49 J. R. Bellare, H. T. Davis, L. E. Scriven and Y. Talmon, *J. Electron Microsc. Tech.*, 1988, **10**, 87.
50 H. Edlund, A. Khan and C. La Mesa, *Langmuir*, 1998, **14**, 3691.
51 E. F. Marques, H. Edlund, C. La Mesa and A. Khan, *Langmuir*, 2000, **16**, 5178.
52 H. Amenitsch, H. Edlund, A. Khan, E. F. Marques and C. La Mesa, *Colloids Surf., A*, 2003, **213**, 79.
53 P. Terech, B. Jean and F. Ne, *Adv. Mater.*, 2006, **18**, 1571.
54 M. Gubitosi, L. Travaglini, M. C. di Gregorio, N. V. Pavel, J. Vázquez Tato, S. Sennato, U. Olsson, K. Schillén and L. Galantini, *Angew. Chem., Int. Ed.*, 2015, **54**, 7018.
55 H. Sugioka, K. Matsuoka and Y. Moroi, *J. Colloid Interface Sci.*, 2003, **259**, 156.
56 R. Ninomiya, K. Matsuoka and Y. Moroi, *Biochim. Biophys. Acta*, 2003, **1634**, 116.
57 M. L. Bhaisare, S. Pandey, M. S. Khan, A. Talib and H.-F. Wu, *Talanta*, 2015, **132**, 572.
58 L. Onsager, *Ann. N. Y. Acad. Sci.*, 1949, **51**, 627.
59 R. A. L. Jones, *Soft Condensed Matter*, 123 Oxford University Press, 2002.
60 A. Stroobants, H. N. W. Lekkerkerker and T. Odijk, *Macromolecules*, 1986, **19**, 2232.